CrystEngComm

Accepted Manuscript

ROYAL SOCIETY OF CHEMISTRY

www.rsc.org/crystengcomm

In Situ Recrystallization of Lanthanide Coordination Polymer: From 1D Ladder Chain to 1D Linear Chain

Jing-Wen Sun, Shang-Ju Li, Peng-Fei Yan,* Xu Yao, and Guang-Ming Li*

Key Laboratory of Functional Inorganic Material Chemistry (MOE), School of Chemistry and Materials Science, Heilongjiang University, No. 74, Xuefu Road, Nangang District, Harbin 150080, People's Republic of China

Abstract

Reactions of $LnCl_3 \cdot 6H_2O$ (Ln = La, Ce, Pr, Nd, Gd and Lu), L-dibenzoyl tartaric acid (L-DBTA) and triethylamine in methanol-water solution afford four complexes **1a**–**4a** with 1D ladder chain structures, e.g. $\{[Ln_2(L\text{-}DBTA)_3(CH_3OH)_x(H_2O)_y] \cdot zH_2O\}_n$ (x = 3 or 4, y = 3 or 4, z = 2 or 5; Ln = La (**1a**), Ce (**2a**), Pr (**3a**) and Nd (**4a**)) and two complexes **5** and **6** with 1D linear chain structures, e.g. $\{Et_3NH[Ln(L\text{-}DBTA)_2(CH_3OH)_2(H_2O)_2] \cdot 2H_2O\}_n$ (Ln = Gd (**5**) and Lu (**6**)). Accidently, in situ irreversible SCSC transformation from the kinetically stabilized 1D ladder chain structures of **1a**–**4a** to thermodynamically stabilized 1D linear chain structures of **1**–**4** was observed, which was seldom reported for lanthanide coordination polymers. The coordination stability around lanthanide cation was investigated to expatiate the irreversible SCSC transformation. The solid-state NIR luminescence for complexes **3a**, **3**, **4a** and **4** was also studied.

Introduction

In the scope of solid-state chemical reactions, the recent development of single-crystal-to-single-crystal (SCSC) transformation has attracted extensive interests.[1-3] Most of the transformation is reversible and induced by light and thermal effect.[4, 5] A number of these studies have been reported for organic molecules, inorganic and organometallic compounds, showing that the SCSC transformation of metallo-organic compounds is difficult

in solid-state reactions, because the transformation often engenders a damage for single crystals, especially for those involving an exquisite change of the crystal lattice or cleavage/formation of coordination bonds.[6-14] Recently, SCSC transformation of metallo-organic compounds through in situ recrystallization in the mother liquor has garnered considerable attention, due to that the molecules can move freely so that the reactive functional groups can be brought closer together in the correct orientations for the reaction to take place homogenously.[15-18] The transformation of in situ recrystallization is interconversion between polymorphs or supramolecular isomers.[19] Meta-stable polymorphs (kinetic polymorph) may initially appear and, during the crystallization process, be transformed into more stable polymorphs (thermodynamic polymorph). Such processes may often, but not always, occur because crystallization is a kinetic phenomenon, and a meta-stable polymorph could be locked in for years before one is even aware that there exists a more stable crystal form.[20] However, disassembly of the building blocks of coordination polymeric systems in solution may reduce the conversion barriers and help to transform from meta-stable polymorph to stable one by reassembly.[21-23] This kind of SCSC is actually a thermodynamically controlled recrystallization process following the Ostwald's Rule of Stages.[24, 25] At present, there are a few examples of in situ recrystallization, and the examples mainly focus on transition metal coordination polymers in the realm of molecular crystals.

The interest in the coordination chemistry of L-DBTA (L-dibenzoyl tartaric acid) as ligand has been invigorated in recent years, because the variable coordination modes provided by this carboxyl-rich molecule lead to the isolation of metallo-organic hybrid topologies with multiple metal centers.[26-29] It is thus of considerable interest to investigate whether the polymorphs of the complexes constructed by L-DBTA and lanthanide cations exist and how they assemble. When $LnCl_3 \cdot 6H_2O$ was reacted with L-DBTA in 2:3 molar ratio in methanol-water solution, two types of coordination polymers **1a–4a** featured 1D ladder chain structures and coordination polymers **1–6** featured 1D linear chain structures were obtained, and more significantly, meta-stable phase **1a–4a** can be transformed into stable phase **1–4** in

the mother liquor through dissolution and recrystallization (Scheme 1). The solid-state NIR luminescence investigation revealed complexes **3a**, **3**, **4a** and **4** exhibit the characteristic emission of Pr^{3+} ions and Nd^{3+} ions, respectively. Furthermore, the signal intensities and NIR luminescence life time are changed along with the irreversible SCSC transformation.

Scheme 1 Synthetic routes of complexes **1a**–**4a** and **1**–**6**.

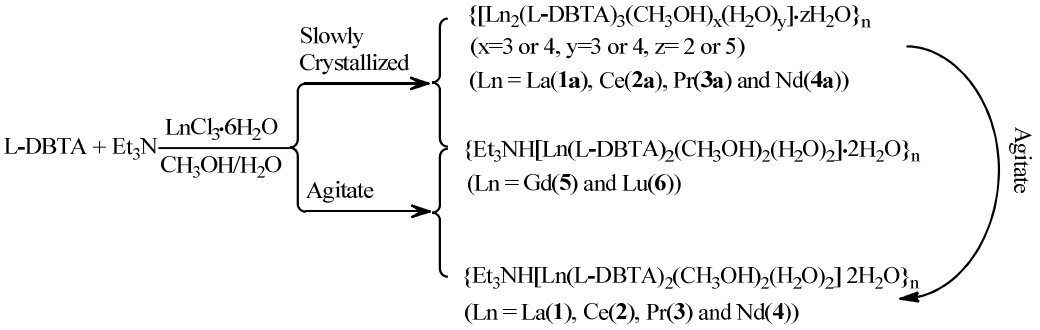

Experimental

All chemicals except $LnCl_3 \cdot 6H_2O$ were obtained from commercial sources and used without further purification. $LnCl_3 \cdot 6H_2O$ were prepared by the reactions of Ln_2O_3 and hydrochloric acid in aqueous solution. Elemental (C, H and N) analyses were performed on a Perkin-Elmer 2400 analyzer. FT-IR data were collected on a Perkin-Elmer 100 spectrophotometer by using KBr pellets in the range of 4000−450 cm^{-1}. UV spectra (in methanol) were recorded on a Perkin-Elmer 35 spectrophotometer. Thermal analyses were carried out on a STA-6000 with a heating rate of 10 °C min^{-1} in a temperature range from 30 °C to 800 °C in N_2 atmosphere. The PXRD have been carried out on a D/MAX-3B X-ray diffractometer with Cu K_α radiation (λ = 1.5406 Å). Excitation and emission spectra were measured with an Edinburgh FLS 920 fluorescence spectrophotometer. NIR lifetimes were recorded on a single photon counting spectrometer from Edinburgh Instrument (FLS 920) with microsecond pulse lamp as the excitation. The data were analyzed by software supplied by Edinburgh Instruments. Single-crystal X-ray data for all complexes were collected on a Rigaku R-AXIS RAPID imaging plate diffractometer with graphite-monochromated Mo Kα (λ = 0.71073 Å) at 293 K.

Empirical absorption corrections based on equivalent reflections were applied. The structures were solved by direct methods and refined by full-matrix least-squares methods on F^2 using SHELXS-97 crystallographic software package. All non-hydrogen atoms are anisotropically refined. All of the crystal data and structure refinement details for complexes are summarized in Table S1.

Preparation of complexes 1a–4a and 1–6

The similar procedures were employed in preparing complexes **1a**−**4a** and **5**−**6** (Scheme 1). In a typical synthesis of **1a**, a methanol solution (8 mL) of L–DBTA (0.358 g, 1.00 mmol) with triethylamine was slowly layered on an aqueous solution (8 mL) of $LaCl_3 \cdot 6H_2O$ (0.233 g, 0.66 mmol) in a test tube. The tube was sealed and stored in darkness at ambient temperature. The colorless needle-like crystals (**1a**−**4a**) and cubic blocks crystals (**5**−**6**) suitable for X-ray diffraction analysis were obtained in about one week. When complex **1a**−**4a** was agitated in mother liquid for several minutes, and then sealed and stored in the same environment for two weeks. The colorless needle crystals were transferred to the cubic blocks crystals of **1**−**4**, respectively.

Synthesis of $\{[La_2(L\text{-}DBTA)_3(CH_3OH)_4(H_2O)_3]\cdot 5H_2O\}_n$ (1a). Yield: 0.240 g, 45 % (based on La). Elemental analysis (%) Calcd for $C_{58}H_{60}La_2O_{32}$ (M_r = 1618.94): C 43.03, H 4.23; Found: C 43.12, H 4.17. IR data (KBr pellet, cm^{-1}): 3441 (s), 1720 (s), 1603 (s), 1452 (m), 1431 (m), 1271 (s), 1120 (s). UV–vis (MeOH, nm): 229, 273, 281.

Synthesis of $\{[Ce_2(L\text{-}DBTA)_3(CH_3OH)_4(H_2O)_3]\cdot 2H_2O\}_n$ (2a). Yield: 0.217 g, 42 % (based on Ce). Elemental analysis (%) Calcd for $C_{58}H_{62}Ce_2O_{33}$ (M_r = 1567.32): C 44.45, H 3.99; Found: C 44.50, H 3.90. IR data (KBr pellet, cm^{-1}): 3441 (s), 1720 (s), 1601 (s), 1452 (m), 1430 (m), 1270 (s), 1122 (s). UV–vis (MeOH, nm): 229, 274, 281.

Synthesis of {[Pr_2(L-DBTA)$_3$(CH_3OH)$_4$(H_2O)$_3$]·5H_2O}$_n$ (3a). Yield: 0.268 g, 50 % (based on Pr). Elemental analysis (%) Calcd for $C_{58}H_{68}Pr_2O_{36}$ (M_r = 1622.94): C 42.92, H 4.22; Found: C 42.85, H 4.31. IR data (KBr pellet, cm^{-1}): 3440s, 1720s, 1602s, 1453m, 1431m, 1271s, 1121s. UV–vis (MeOH, nm): 229, 273, 281.

Synthesis of {[Nd_2(L-DBTA)$_3$(CH_3OH)$_3$(H_2O)$_4$]·2H_2O}$_n$ (4a). Yield: 0.247 g, 48 % (based on Nd). Elemental analysis (%) Calcd for $C_{57}H_{60}Nd_2O_{33}$ (M_r = 1561.53): C 43.84, H 3.87; Found: C 43.80, H 3.91. IR data (KBr pellet, cm^{-1}): 3440 (s), 1720 (s), 1601 (s), 1452 (m), 1432 (m), 1270 (s), 1121 (s). UV–vis (MeOH, nm): 230, 273, 281.

Synthesis of {Et_3NH[La(L-DBTA)$_2$(CH_3OH)$_2$(H_2O)$_2$]·2H_2O}$_n$ (1). Elemental analysis (%) Calcd for $C_{44}H_{56}LaNO_{22}$ (M_r = 1089.81): calcd: C 48.49, H 5.18, N 1.29; Found: C 48.50, H 5.23, N 1.32. IR data (KBr pellet, cm^{-1}): 3490 (s), 1715 (s), 1602 (s), 1452 (m), 1428 (m), 1272 (s), 1121 (s). UV–vis (MeOH, nm): 230, 274, 280.

Synthesis of {Et_3NH[Ce(L-DBTA)$_2$(CH_3OH)$_2$(H_2O)$_2$]·2H_2O}$_n$ (2). Elemental analysis (%) Calcd for $C_{44}H_{56}CeNO_{22}$ (M_r = 1091.02): calcd: C 48.44, H 5.17, N 1.28; Found: C 48.49, H 5.23, N 1.31. IR data (KBr pellet, cm^{-1}): 3494 (s), 1715 (s), 1602 (s), 1452 (m), 1417 (m), 1270 (s), 1119 (s). UV–vis (MeOH, nm): 229, 273, 280.

Synthesis of {Et_3NH[Pr(L-DBTA)$_2$(CH_3OH)$_2$(H_2O)$_2$]·2H_2O}$_n$ (3). Elemental analysis (%) Calcd for $C_{44}H_{56}PrNO_{22}$ (M_r = 1091.80): calcd: C 48.40, H 5.17, N 1.28; Found: C 48.49, H 5.23, N 1.31. IR data (KBr pellet, cm^{-1}): 3491 (s), 1715 (s), 1602 (s), 1452 (m), 1427 (m), 1272 (s), 1120 (s). UV–vis (MeOH, nm): 229, 273, 281.

Synthesis of {Et_3NH[Nd(L-DBTA)$_2$(CH_3OH)$_2$(H_2O)$_2$]·2H_2O}$_n$ (4). Elemental analysis (%) Calcd for $C_{44}H_{56}NdNO_{22}$ (M_r = 1095.14): calcd: C 48.40, H 5.17, N 1.28; Found: C 48.49, H 5.23, N 1.31. IR data (KBr pellet, cm^{-1}): 3494 (s), 1715 (s), 1602 (s), 1452 (m), 1424 (m), 1271 (s), 1121 (s). UV–vis (MeOH, nm): 229, 274, 280.

Synthesis of $\{Et_3NH[Gd(L\text{-}DBTA)_2(CH_3OH)_2(H_2O)_2]\cdot 2H_2O\}_n$ (5). Yield: 0.336 g, 46 %. Elemental analysis (%) Calcd for $C_{44}H_{56}GdNO_{22}$ (M_r = 1108.15): C 47.69, H 5.09, N 1.26; Found: C 47.60, H 5.17, N 1.24. IR data (KBr pellet, cm^{-1}): 3503 (s), 1717 (s), 1602 (s), 1452 (m), 1271 (m), 1271 (s), 1121 (s). UV–vis (MeOH, nm): 230, 273, 281.

Synthesis of $\{Et_3NH[Lu(L\text{-}DBTA)_2(CH_3OH)_2(H_2O)_2]\cdot 2H_2O\}_n$ (6). Yield: 0.201 g, 27 %. Elemental analysis (%) Calcd for $C_{44}H_{56}LuNO_{22}$ (M_r = 1125.87): C 46.94, H 5.01, N 1.24; Found: C 47.03, H 5.10, N 1.27. IR data (KBr pellet, cm^{-1}): 3494 (s), 1718 (s), 1602 (s), 1452 (m), 1427 (m), 1271 (s), 1121 (s). UV–vis (MeOH, nm): 230, 273, 280.

X-ray Crystallography

Crystal dates of complexes **1a–4a** and **1–6** were selected on an Oxford Xcalibur Gemini Ultra diffractometer using graphite-monochromated Mo-Kα radiation (λ = 0.71073 Å) at room temperature. Structures of **1a–4a** and **1–6** were solved using Patterson methods (SHELXS-97), expanded using Fourier methods and refined using SHELXL-97 (full-matrix least-squares on F^2) and WinGX v1.70.01 programs packages.[30-32] In complexes **1a–4a** and **1–6**, the contribution of HIGHLY disordered anions/solvent molecules were treated as diffuse using the Squeeze procedure implemented in the Platon program.[33, 34] The resulting new files were used to further refine the structures. The Squeeze results are consistent with TG and elemental analysis, which indicate that there are five water molecules as free guests in complexes **1a** and **3a**, two water molecules as free guests in complexes **2a, 3a** and **1-6**, respectively. These water molecules were added in the molecular formula. During the refinement, the commands "ISOR" and "DELU" were used to restrain the non-H atoms with ADP and NPD problems, and these detailed operations were listed in the CIF files. All non-hydrogen atoms were refined anisotropically. Empirical absorption corrections based on equivalent reflections were applied. The crystal data and structure refinements of complexes **1a–4a** and **1–6** are summarized in Table 1. Selected bond lengths and angles for complexes **1a–4a** and **1–6** are listed in Tables S2. Crystallographic data for the structures reported in this

paper have been deposited in the Cambridge Crystallographic Data Center with CCDC No. 723332, 723334, 723336, 848922, 859164, 859165, and 855715−855718.

Results and discussion

Synthesis

The reactions of $LnCl_3 \cdot 6H_2O$ with L-DBTA in a 2:3 molar ration in a CH_3OH-H_2O solution in the presence of triethylamine afforded strip-like crystals **1a–4a** (La (**1a**), Ce (**2a**), Pr (**3a**) and Nd (**4a**)) and block-like crystals **5** and **6** (Gd (**5**) and Lu (**6**)) in one month. Notably, complexes **1a–4a** exhibit distinct crystal morphology in contrast to that for complexes **5** and **6** under the similar synthesis conditions. One response is from the lanthanide contraction and another may originate from polymorphism or supramolecular isomerism.[20] According to Ostwald's Rule of Stages, in a polymorphic system, the meta-stable compounds can form in the beginning of the reaction and will be transformed into the thermodynamically stable compounds as a function of time.[24] When the energy barrier is high between metastable and thermodynamically stable compounds, the isolation of thermodynamically stable compounds are difficult. However, the transformation for complexes **1a–4a**, **5** and **6** can't occur in a quite long period. To prompt the process, the crystals of complexes **1a**–**4a**, **5** and **6** were agitated in the mother solution. As a result, complexes **1a**–**4a** with strip-like crystals dissolved and recrystalized as block-like crystals of **1**–**4** in about two weeks, suggesting that complexes **1**–**4** be more thermodynamically stable one (Fig. 1). It illustrates an interesting transformation from a kinetically favored crystalline phase (i.e., **1a**–**4a**) to a more thermodynamically stable phase (i.e., **1**–**4**) through crystal dissolution and recrystallization by agitation, in which the two phase possess high energy barrier. When **1**–**4** are suspended in the mother liquor for weeks, they remain stable, indicating that the **1a**–**4a** → **1**–**4** transformation is irreversible. In addition, the formation of the meta-stable complexes is strongly dependent on the lanthanide cations. Only light lanthanide cations such as La^{3+}, Ce^{3+}, Pr^{3+}, and Nd^{3+} with a large ionic radius could generate the meta-stable complexes. The preparation process represents a rare

example of spontaneous rearrangement partly dictated by the nature of the lanthanide cations.

Characterization. The FT-IR spectra of complexes **1a**–**4a** and **1**–**6** exhibit similar patterns (Fig. S3). In a typical spectrum of complex **1a**, the broad band around 3441 cm^{-1} is attributed to the characteristic peak of O-H bonds from the solvent molecules in the complex. The asymmetric stretching vibrations of carboxylate groups are observed at 1702, 1603, 1452, and 1431 cm^{-1}. The appearance of the characteristic band at 1603 cm^{-1} indicates the deprotonation of the carboxylate groups and coordination to the lanthanide ions. The UV-vis absorption data of L-DBTA, **1a**–**4a** and **1**–**6** were conducted in methanol solution and exhibit a similar pattern (Fig. S4). The main absorption bands at *ca.* 230 nm are attributed to the π-π* transitions of benzene ring. And two weak absorption at *ca.* 273 nm and 281 nm, which are assigned to the π-π* and n-π* transitions of benzene ring. The PXRD patterns for **1a**–**4a** and **1**–**6** are presented in Fig. S5. The diffraction peaks of both the simulated and experimental patterns match well, indicating that the phase purity of the complexes are good. The thermal stabilities of all complexes **1a**–**4a** and **1**–**6** are investigated by TG-DSC analysis (Fig. S6–S15). All complexes **1a**–**4a** starts to release the coordinated solvents and lattice solvents from 303 K to 378 K, and no further weight loss was found until about 465 K. Then the decomposition commence. While, all complexes **1**–**6** start to lose the coordinated solvent and lattice solvents in the same range of 303 K to 365 K but no further weight loss was found till about 419 K. The weight loss of coordinated solvents and lattice solvents agree with the calculated value for all complexes.

Crystal Structure of 1a–4a. The single-crystal X-ray diffraction analysis reveals that complexes **1a**–**4a** are isomorphic. In a typical structure of complexes **1a**–**4a**, complex **1a** crystallizes in monoclinic chiral space group $P2_1$ featuring 1D ladder-like type framework. The asymmetric unit of **1a** contains two independent La(III) cations, three independent L-$DBTA^{2-}$ anions, two coordinated water molecules, two methanol molecules, and five lattice water molecules (Fig. 1). The La1(III) cation is nine-coordinated in a tri-capped trigonal

prism geometry defined by five O atoms (O3, O4, O5, O11 and O22) from four acetates of four L-DBTA ligands, two O atoms (O25 and O27) from two methanol molecules and two O atoms (O26 and O31) from two water molecules, with La–O bond distances of 2.417–2.753 Å. The La2(III) cation displays the similar geometry with La1(III), the geometry coordinated by six O atoms (O4, O12, O13, O19, O21 and O22) from five acetates of four L-DBTA ligands, two O atoms (O28 and O30) from two methanol molecules and one O atom (O29) from one water molecule, with La–O bond distances of 2.446–2.817 Å. Additionally, there are three types of L-DBTA ligands (A-, B- and C-type) in complex **1a** (Fig. 2). Both of A-type and B-type ligands take (κ^1-κ^1-μ_2)-(κ^1)-μ_2, while C-type take (κ^1-κ^2-μ_2)-(κ^1)-μ_3. Firstly, A-type and B-type ligands adopt both bridging and chelating mode to link Ln1(III) and Ln2(III) cations, which result in a 1D ladder chain (Fig. S1). Furthermore, the C-type ligand bind to the Ln(III) cations on the chain to form a more stable 1D ladder chain (Fig. 3 left).

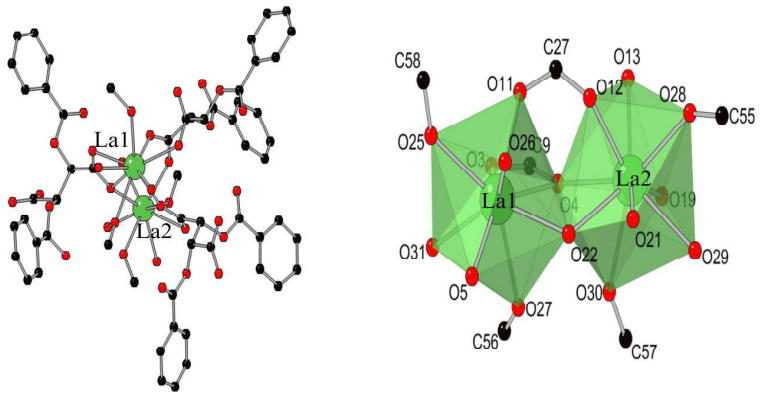

Fig. 1 Combined ball and stick representations of the molecular structure unit of **1a** and the coordination environments of La(III) cations.

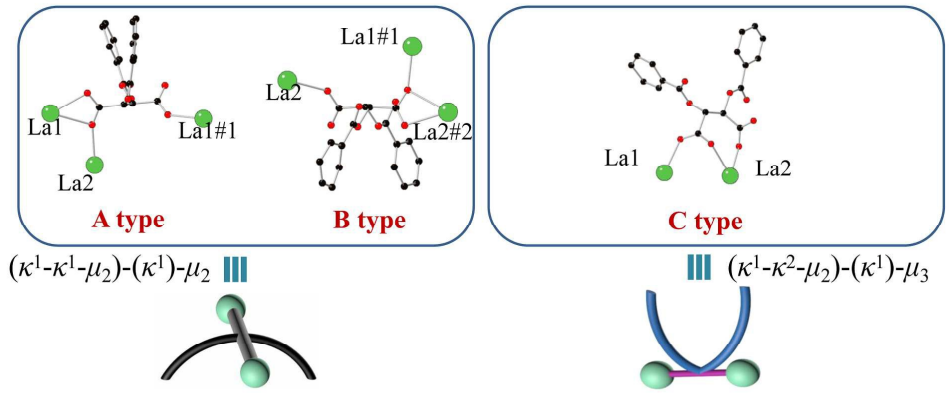

Fig. 2 Three types of L–DBTA^{2-} anions in complex **1a**.

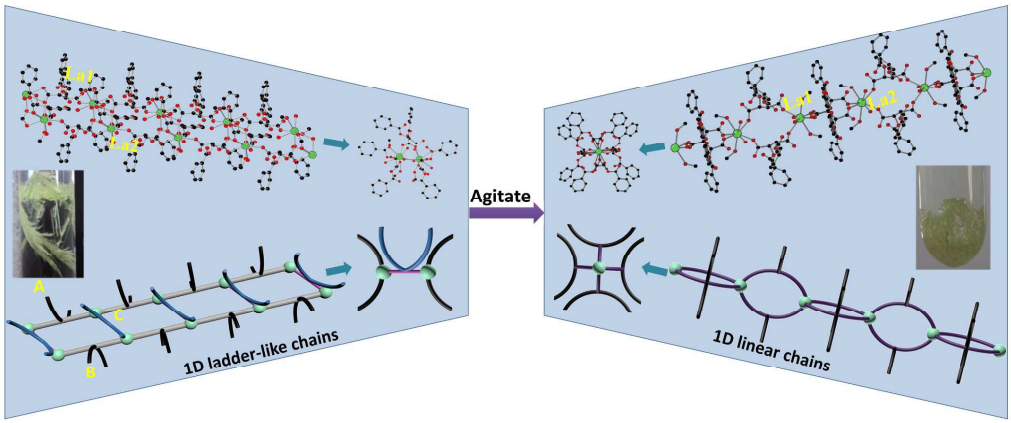

Fig. 3 (left) Combined ball/stick and cartoon representations of 1D ladder chain in complex **1a**; (right) the representations of 1D ladder chain in complex **1**. The insert pictures show the side view of 1D chains. All solvent molecules are omitted for clarity. La, green; O, red; C, black. Photograph are image highlighting the in situ recrystallization of **1a–4a** to **1–4** in the mother liquor.

Crystal Structure of 1–6. The single-crystal X-ray diffraction analysis reveals that complexes **1–6** are isomorphic. In a typical structure of complexes **1–6**, complex **1** crystallizes in monoclinic chiral space group $P2_12_12$ featuring 1D linear type framework. The asymmetric unit of **1** contains two half independent La(III) cations, two independent L-DBTA^{2-} anions, two coordinated water molecules, two methanol molecules, one trimethylamine molecule and two lattice water molecules (Fig. 4). The La1(III) cation is eight-coordinated in a di-capped trigonal prism geometry defined by five O atoms (O8, O8#1, O16 and O16#1) from four acetates of four L-DBTA ligands, two O atoms (O17 and O17#1) from two methanol molecules and two O atoms (O18 and O18#1) from two water molecules,

with La–O bond distances of 2.446–2.591 Å. The La2(III) cation displays the similar geometry with La1(III), the geometry coordinated by six O atoms (O4#2, O4#3, O12 and O12#1) from four acetates of four L-DBTA ligands, two O atoms (O20 and O20#1) from two methanol molecules and two O atoms (O19 and O19#1) from two water molecules, with La–O bond distances of 2.447–2.531 Å. In complex **1**, there are two types of L-DBTA ligands, which both take (κ^1)-(κ^1)-μ_2 coordination mode (Fig. S2). The Ln1(III) and Ln2(III) cations are linked by the two types of L-DBTA ligands to form a 1D linear chain (Fig. 3 right).

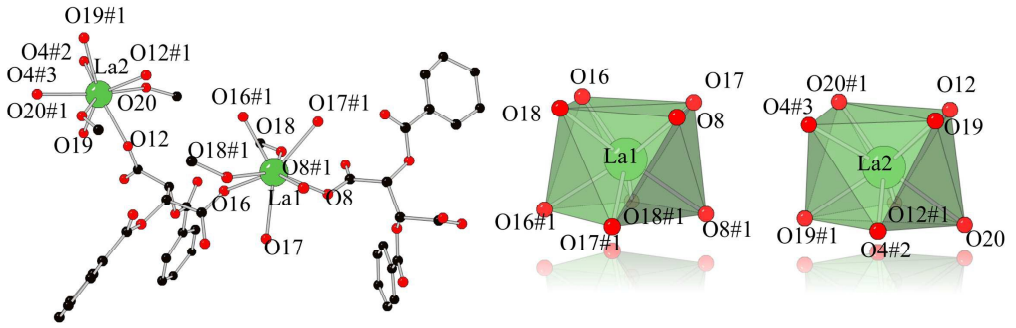

Fig. 4 Combined ball and stick representations of the molecular structure unit of **1** and the coordination environments of La(III) cations. (symmetry code: #1 1-x, 2-y, z; #2 x, y, -1+z; #3 1–x, 2-y, -1+z)

In comparison with the structures of **1a**–**4a** and **1**–**4,** the cleavage of interchain Ln–O coordination bonds that simultaneously induce the crystal transformation with the chain rearrangement in complexes **1a**–**4a** (Fig. 5). The nine-coordinated distorted tri-capped trigonal prism geometry for all La(III) cations in **1a** is changed to eight-coordinated anti-quadrangular geometry for all La(III) cations in **1**. In addition, the average bond length of Ln–O is shrinked from 2.560 Å in **1a** to 2.512 Å in **1** suggesting that **1** is more stable than **1a**. Obviously, this significant changes in bond length are attributed to the transformation of in situ recrystallization, which the molecules can move freely so that the reactive functional groups can be brought closer together in the correct orientations for the reaction to take place homogenously.

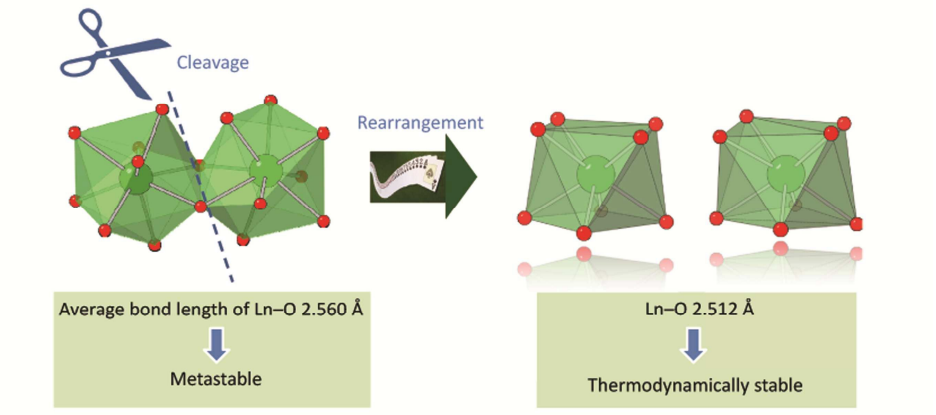

Fig. 5 Combined ball/stick/polyhedra and cartoon representations of the cleavage of interchain Ln–O coordination bonds.

NIR Properties. The emission spectrum of the Pr(III) complexes **3a** and **3** in the NIR region (Fig. 6) shows three emission bands at 898, 1049, and 1497 nm, which can be assigned as $^1D_2 \rightarrow {}^3F_2$, $^1D_2 \rightarrow {}^3F_2$, and $^1D_2 \rightarrow {}^1G_4$, respectively. The luminescent spectra of Pr^{3+} ion are more complicated compared with other lanthanide ions, since the Pr^{3+} ion can show emissions from three different levels ($^3P_0$, $^1D_2$ and $^1G_4$) when the complexes are excited. The emitting peaks at 1049 nm originate from $^1D_2$, not $^1G_4$ level,[35] because the lack of the NIR emission at about 1320 nm corresponding to $^1G_4 \rightarrow {}^3H_5$ implies the relaxation of $^1G_4$ manifold energy levels. It is attractive to design sensitizers whose triplet state can match the energy level of the receiving lanthanide ion in order to obtain the efficient energy transfer. The L-DBTA ligand can match well with the $^1D_2$ level of Pr^{3+} ion, and an efficient energy transfer can occur between the L-DBTA and the Pr^{3+}, followed by the observation of the efficient NIR emission. The signal intensities of complex **3a** are stronger than that of complex **3**. Correspondingly, the NIR luminescence life time for complex **3a** (τ_1 = 1.73 μs) are longer than complex **3** (τ_1 = 1.51 μs) (Fig. S18). It is attributed to less solvent molecules coordinated to the Pr^{3+} ions in **3** than that in **3a** quenching the NIR luminescence. The solid-state NIR spectra of complexes **4a** and **4** exhibit the characteristic emission of Nd^{3+} ions (Fig. 6), respectively, which is attributed to the efficient ligand-to-lanthanide energy transfer. The emission peak patterns for complexes **4a** and **4** are similar and corresponding to the transitions from $^4F_{3/2} \rightarrow {}^4I_{9/2}$ at 909 nm,

$^4F_{3/2}\rightarrow{}^4I_{11/2}$ at 1054 nm and $^4F_{3/2}\rightarrow{}^4I_{13/2}$ at 1266 nm. Note that the emission band of Nd^{3+} ion is not a single sharp transitions at 909 nm, rather it appears as mountain peaks of bands arising at lower and higher energies, which is attributed to the crystal field splitting and stark splitting. Similar splitting about Yb^{3+} complexes has been reported previously.[36] Similar as complexes **3** and **3a**, the signal intensities of complex **4a** are stronger than that of complex **4**. The NIR luminescence life time for complex **4a** (τ_1 = 1.07 μs, τ_2 = 5.82 μs) are longer than complex **4** (τ_1 = 0.88 μs, τ_2 = 6.19 μs) (Fig. S18). However, we are not able to give quantitative expatiation at current stage.

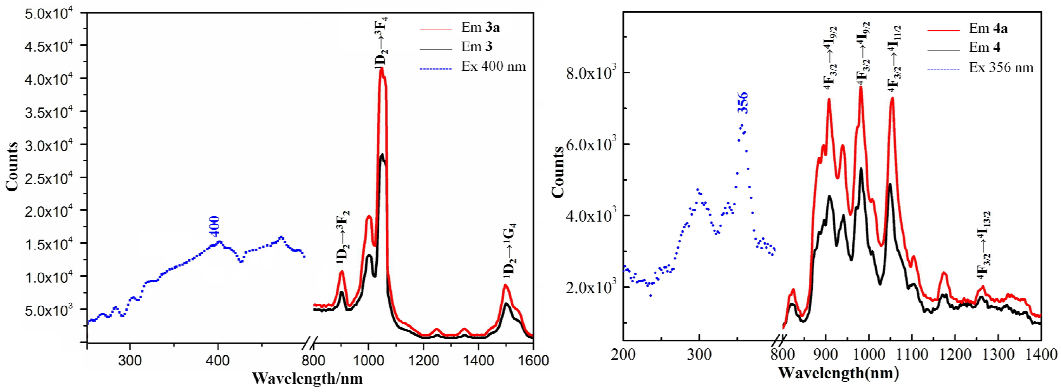

Fig. 6 NIR photoluminescence of complexes **3a**, **3**, **4a** and **4** in the solid state at 193 K.

Conclusions

Isolation and characterization of complexes **1a**–**4a** and **1**–**6,** demonstrate that L-dibenzoyl tartaric acid (L-DBTA) is able to react with $LnCl_3\cdot 6H_2O$ affording 1D ladder and 1D linear chain structures depending on the reaction conditions. Notably, the radii of the lanthanide cations play a crucial role on affording the kinetically stabilized 1D ladder complexes **1a**–**4a**. The coordination stability around lanthanide cations dominates the in situ irreversible SCSC transformation from the kinetically stabilized 1D ladder chain structure of **1a**–**4a** to the thermodynamically stabilized 1D linear chain structure of **1**–**4**. NIR luminescence for complexes **3a**, **3**, **4a** and **4** verifies that complexes **3a** and **4a** with relatively ridged structure sand encaged lanthanide cations exhibit strong luminescence and longer life time than that for

complex **3** and **4**. This work represents a rare example of in situ irreversible SCSC transformation for lanthanide coordination polymers.

Acknowledgements

This work is financially supported by the National Natural Science Foundation of China (No. 21471051, 51472076, 21271089 & 51473046).

† Electronic supplementary information (ESI) available: crystallographic, IR, TGA, PXRD data, and additional figures. For ESI and crystallographic data in CIF or other electronic format see DOI:

Notes and references

(1) Y.-M. Song, F. Luo, M.-B. Luo, Z.-W. Liao, G.-M. Sun, X.-Z. Tian, Y. Zhu, Z.-J. Yuan, S.-J. Liu, W.-Y. Xu, X.-F. Feng, *Chem. Commun.*, 2012, **48**, 1006.

(2) Y.-C. Ou, W.-T. Liu, J.-Y. Li, G.-G. Zhang, J. Wang, M.-L. Tong, *Chem. Commun.*, 2011, **47**, 9384.

(3) G. K. Kolea, J. J. Vittal, *Chem. Soc. Rev.*, 2013, **42**, 1755.

(4) J. P. Zhang, Y. Y. Lin, W. X. Zhang, X. M. Chen, *J. Am. Chem. Soc.*, 2005, **127**, 14162.

(5) J. Seo, R. Matsuda, H. Sakamoto, C. Bonneau, S. Kitagawa, *J. Am. Chem. Soc.*, 2009, **131**, 12792.

(6) A. Natarajan, C. K. Tsai, S. I. Khan, P. McCarren, K. N. Houk, M. A. Garcia-Garibay, *J. Am. Chem. Soc.*, 2007, **129**, 9846.

(7) H. Sadeghzadeh, A. Morsali, *Inorg. Chem.*, 2009, **48**, 10871.

(8) D. M. Kelly, K. S. Eccles, C. J. Elcoate, S. E. Lawrence, H. A. Moynihan, *Cryst. Growth Des.*, 2010, **10**, 4303.

(9) K. Uehara, N. Mizuno, *J. Am. Chem. Soc.*, 2011, **133**, 1622.

(10) Y. Fu, J. Su, S.-H. Yang, Z.-B. Zou, G.-B. Li, F.-H. Liao, M. Xiong, J.-H. Lin, *Cryst. Growth Des.*, 2011, **11**, 2243.

(11) Z.-M. Duan, Y. Zhang, B. Zhang, D.-B. Zhu, *J. Am. Chem. Soc.*, 2009, **131**, 6934.

(12) M.-L. Sun, L. Zhang, Q.-P. Lin, J. Zhang, Y.-G. Yao, *Cryst. Growth Des.*, 2010, **10**, 1464.

(13) P. B. Chatterjee, A. Audhya, S. Bhattacharya, S. M. T. Abtab, K. Bhattacharya, M. Chaudhury, *J. Am. Chem. Soc.*, 2010, **132**, 15842.

(14) X.-D. Zheng, M. Zhang, L. Jiang, T.-B. Lu, *Dalton Trans.*, 2012, **41**, 1786.

(15) J. Vittal, J. *Coord. Chem. Rev.*, 2007, **251**, 1781.

(16) C. H. Hu, U. Englert, *Angew. Chem. Int. Ed.*, 2005, **44**, 2281.

(17) Y. L. Bai, J. Tao, R. B. Huang, L. S. Zheng, *CrystEngComm*, 2008, **10**, 472.

(18) X. Liu, H. Y. An, Z. F. Chen, H. Zhang, Y. Hu, G. B. Zhu, Y. V. Geletii, C. L. Hill, *Eur. J. Inorg. Chem.*, 2013, 1827.

(19) J.-P. Zhang, X.-C. Huang, X.-M. Chen, *Chem. Soc. Rev.*, 2009, **38**, 2385.

(20) G. R. Desiraju, *Angew. Chem. Int. Ed.*, 2007, **46**, 8342.

(21) C. Näther, G. Bhosekar, I. Jess, *Inorg. Chem*., 2007, **46**, 8079.

(22) M.-L. Tong, S. Hu, J. Wang, S. Kitagawa, S. W. Ng, *Cryst. Growth Des.*, 2005, **5**, 837.

(23) X.-R. Wu, X. Yang, R.-J. Wei, J. Li, L.-S. Zheng, J. Tao, *Cryst. Growth Des.*, 2014, **14**, 4891.

(24) W. Z. Ostwald, *Phys. Chem.*, 1897, **22**, 289.

(25) J. Tao, R.-J. Wei, R.-B. Huang, L.-S. Zheng, *Chem. Soc. Rev*., 2012, **41**, 703.

(26) Y.-F. Han, X.-Y. Li, L.-Q. Li, Ma, Z. Shen, Y. Song, X.-Z. You, *Inorg. Chem.*, 2010, **49**, 10781.

(27) R. Feng, F.-L. Jiang, M.-Y. Wu, L. Chen, C.-F. Yan, M.-C. Hong, *Cryst. Growth Des.*, 2010, **10**, 2306.

(28) X.-J. Wang, Z.-M. Cen, Q.-L. Ni, X.-F. Jiang, H.-C. Lian, L.-C. Gui, H.-H. Zuo, Z.-Y. Wang, *Cryst. Growth Des.*, 2010, **10**, 2960.

(29) C. Feng, J.-W. Sun, P.-F. Yan, Y.-X. Li, T.-Q. Liu, Q.-Y. Sun, G.-M. Li, *Dalton Trans.*, 2015, **44**, 4640.

(30) G. M. Sheldrick, *Program for Structure Refinement*: University of Göttingen, Germany, 1997.

(31) L. Farrugia, *J. Appl. Cryst*., 1999, **32**, 837.

(32) Sheldrick, G. M. *SHELXL-97* (1997) Program for the Refinement of Crystal.

(33) Sheldrick, G. M. *ActaCryst*., 1990, **A46**, 467.

(34) Sheldrick, G. M. *ActaCryst*., 2008, **A64**, 112.

(35) A. I. Voloshin, N. M. Shavaleev, V. P. Kazakov, *J. Lumin*., 2001, **93**, 199.

(36) T.-S. Kong, B. S. Harrison, M. Bouguerraya, T. J. Foley, J. M. Boncella, K. S. Schanze, Reynolds, *Adv. Funct. Mater.*, 2003, **13**, 205.

Graphic Abstract

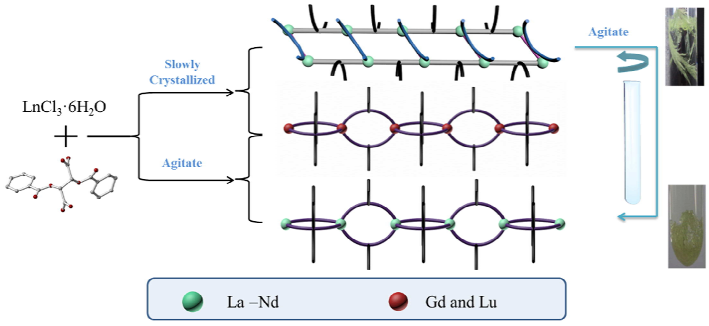

A scarce SCSC transformation for lanthanide coordination polymers are triggered by solvent-mediated isomerization.